*Article*

# Influence and Mechanism Study of Soil Moisture on the Stability of Arsenic-Bearing Ferrihydrite in Surface Soil Vertical Profiles

Lijuan Li [1,2], Xinyi Chen [2], Yan Wang [2], Fubin Zhang [2,*], Xinyi Zhou [2] and Tuo Zhang [3,*]

[1] Institute of Agricultural Environment and Sustainable Development, Chinese Academy of Agriculture Sciences, Beijing 100081, China; liljuan96@163.com
[2] College of Environmental Science & Engineering, China West Normal University, Nanchong 637009, China; chenxy0902@126.com (X.C.); threefire72@163.com (Y.W.); zhouxinyi2024@126.com (X.Z.)
[3] School of Environmental and Life Science, Nanning Normal University, Nanning 530100, China
* Correspondence: sczhangfubin@163.com (F.Z.); xiaotuodujiang@126.com (T.Z.)

**Abstract:** Ferrihydrite is usually used as a remedy for arsenic (As)-contaminated soil due to its strong affinity and large specific surface area. However, its noncrystalline phase makes it unstable in long-term applications in the soil. In this study, a soil incubation experiment was designed using the diffusive gradient in thin film (DGT) technique and spectral techniques to investigate the fate of As-bearing ferrihydrite [As(V)-Fh] after long-term incubation at different soil water holding capacities (SWHCs). After As(V)-Fh (0.05 and 0.005 As/Fe molar ratio) was incubated in soil for 360 days, both DGT-derived labile As and Fe were released at 70% SWHC and 120% SWHC into the soil (at a vertical depth of 12 cm). The concentrations of DGT-As and DGT-Fe increased with incubation time and were greater at 120% SWHC. The results of X-ray diffraction (XRD) and scanning electron microscopy (SEM) showed that As(V)-Fh gradually transformed into hematite and goethite after 360 days of incubation. Goethite was mainly found in the 120% SWHC treatment after 180 days. Hematite and goethite formation rates were greater in the 120% SWHC treatment and in the bottom soil layer. Mechanistic analysis based on X-ray photoelectron spectroscopy (XPS) revealed that the variation in soil pH and the formation of Fe(II) (under flooded water conditions) are the two key factors promoting the formation of hematite (dehydrogenation and dehydration) and goethite (As(V)-Fh dissociation and reorganization). The As release mainly occurred due to the loss of adsorption sites. Thus, it is recommended that ferrihydrite be applied in paddy–dry rotations or dry-field patterns to effectively avoid the loss of As(V)-Fh in long-term-saturated soil.

**Keywords:** As; ferrihydrite; DGT; transformation; SWHC

## 1. Introduction

Arsenic (As) is a widespread, highly toxic metal(loid) element found in natural and contaminated environments [1–3]. As exposure occurs through two main pathways: natural activities (volcanic eruptions and rock weathering) and anthropogenic activities (industrial and agricultural activities) [4,5]. As has strong ecotoxicity and has been listed as a carcinogen by the International Agency for Research on Cancer (IARC) and the World Health Organization (WHO) [6,7]. Statistics show that approximately 19 countries in the world are currently suffering serious As pollution, and China is one of the countries with the most severe As pollution [8]. The "National Soil Pollution Investigation Bulletin", issued by the Ministry of Ecology and Environment and the Ministry of Land and Resources of China in 2014, reported that the exceedance rate of As in Chinese soil was 2.7%, and the heavy pollution ratio was 0.1%, ranking As as an element of serious concern (cadmium was ranked first). The questions of how to control the bioavailability of As in soil and how to avoid the transport of As into crops are major challenges in China.

In the soil environment, As normally undergoes dynamic biogeochemical processes such as adsorption/desorption, coprecipitation/dissolution, and oxidation/reduction [9,10].

In this process, iron (hydr)oxide redox cycling plays a role in controlling As mobility by transformation or reductive dissolution into a new form [11]. Thus, iron (hydr)oxides are widely used as robust amendments for controlling the lability of As in different soil environments [12,13]. Ferrihydrite is an iron oxide widely distributed in soils, sediments, and surface waters [14]. Iron oxide is generally recognized as the iron oxide with the best As adsorption effect among the previously studied Fe(III) (hydr)oxides (ferrihydrite, goethite, lepidocrocite, magnetite, and hematite) due to its nanoscale size, high specific surface area, and strong binding affinity [15]. Nevertheless, controversy regarding its effect on As adsorption still exists as a result of its unstable noncrystalline amorphous structure. Several researchers have shown that the transformation of As-bearing ferrihydrite enhances the adsorption of As by the new iron phase [16–18], while other researchers have shown that transformation or reductive dissolution may induce the release of As into aqueous systems [19,20]. The above controversy mainly derives from the different aqueous systems used by researchers, which makes it challenging to determine the appropriate experimental conditions for assessing the application of ferrihydrite as an effective soil amendment. At present, limited work has been conducted on the fate of As-bearing ferrihydrite during long-term soil incubation. Therefore, the issues of how the stability of ferrihydrite changes in saturated or unsaturated soil and how the lability of As changes during the potential transformation process of ferrihydrite still need to be clarified. Thus, a systematic study of the transformation and fate of As-bearing ferrihydrite in soil systems (unsaturated or saturated) may be highly important for evaluating and predicting whether ferrihydrite is a robust option for controlling the mobility of As.

Currently, studies on the dissolution/transformation of iron minerals have generally focused on pure aqueous systems, and few studies have been conducted in real soil environments. This lack of focus mainly occurs because the presence of homogeneous minerals may hinder the observation of the target iron minerals, and it is difficult to predict the mineral dissolution process. However, studies conducted in real soil environments could reveal the more authentic restoration of the geochemical process of ferrihydrite or As(V)–ferrihydrite. To address these limitations, this study innovatively designed a buried nylon bag soil experiment to characterize the transformation of As(V)-Fh via spectral techniques. In addition, unlike in aqueous solution systems, using only the concentrations of Fe and As in soil aqueous solution extracted via traditional chemical extraction methods is also inaccurate for predicting the dissolution of labile Fe and As from the As(V)-Fh surface. The diffusive gradient in thin film (DGT) technique has been widely recognized as a robust tool for studying the behavior of elements in soil, water, and sediment. Compared with traditional chemical extraction methods, in situ DGT measurements can avoid the adverse effects of ex situ sampling processes, and DGT results account for all environmental factors (e.g., pH, temperature, and ionic strength). Thus, DGT can accurately predict the remobilization of Fe and As from As(V)-Fh during the dissolution process.

Red soil is a widespread soil type in southern China. In the red soil regions of Hunan, Guangxi, Guangdong, and Jiangxi provinces, As pollution is widespread and causes a series of public health problems. Due to the richness of iron in red soil, iron oxides are usually the optimal choice for As remediation. In addition, considering that southern China is the main rice production region and experiences a long rainy season, its soil may remain saturated in the long term. On the basis of the above reasons, we think it is necessary to evaluate the behavior of As-bearing ferrihydrite in red soil environments under different soil moisture levels and investigate the potential transformation mechanism involved. Thus, the aims of this study are (1) to use spectral techniques (XRD, SEM, and XPS) to evaluate the effect of soil moisture on As-bearing ferrihydrite transformation, (2) to use DGT to elucidate the redistribution of As in the soil–mineral sphere during As-bearing ferrihydrite transformation processes, and (3) to illuminate the possible factors and mechanisms that influence As-bearing ferrihydrite transformation.

## 2. Materials and Methods

### 2.1. Study Area and Soil Sample Collection

Topsoil samples (0–20 cm) were collected from Shimen, Hunan Province, China (29°02′ N, 111°41′ E). The soil type was that of Argi-Dystric Acrisols. Shimen used to contain the largest realgar mine in Asia, and this region has a long history of As mining. Previously published works reported long-term As pollution in local farmland soil [21,22]. Although some measurements have been carried out by the government to address the problem of As contamination in soil, most As-contaminated farmland near mines is used to cultivate rice or leafy vegetable crops. Surface soil samples (0–20 cm) without As contamination were collected 10 km from the As mine in Shimen County. The soil samples were air-dried, mixed, ground through a 2 mm sieve, and stored in separate polyethylene containers for later use. The methods used to analyze the soil physical and chemical properties are described in Text S1 (Supplementary Materials) [23,24], and the results are shown in Table S1 (Supplementary Materials).

### 2.2. Chemicals

The chemicals used in the present study were purchased from Aladdin Chemical Company, Ltd., Shanghai, China. All the chemicals were of analytical grade and were utilized without further purification. Milli-Q ultrapure water (18.2 MΩ cm) was used for all the experiments.

### 2.3. Synthesis of As(V)-Bearing Ferrihydrite

The synthesis of As(V)-bearing ferrihydrite followed the description of Zhang et al. [25]. The details are described in Text S2 [21,26].

### 2.4. Incubation of As(V)-Fh in Soil

The experimental device used for testing is shown in Figure S1 (Supplementary Materials). For cultivation, the soil was placed in a column made of plexiglass with a height of 25 cm and a width of 8 cm. The total soil depth was approximately 15 cm. A 12 cm long × 1 cm wide 400-mesh-aperture nylon bag (allowing soil solution and free ions to pass through) was prepared by sealing three edges with a plastic-sealing machine. The nylon bag was filled with As(V)-Fh from the top of the nylon bag, after which the nylon bag was cut to a thickness of 2 mm. A red rope was tied onto the top of the nylon bag and passed through the soil layer, which allowed us to determine the position of the nylon bag in the soil column.

Soil was first added to the container up to a depth of 2.5 cm, and the As(V)-Fh-containing nylon bag was then vertically buried in the soil column. Finally, the bag was covered by a 2.5 cm layer of soil at the top. Thus, we finally obtained a soil incubation system consisting of a nylon bag with As(V)-Fh that was buried in soil with a 2.5 cm soil layer to the top and bottom of the column. After the above work was completed, deionized water was added at different soil water holding capacities (SWHCs) (70% and 120% SWHC) to control the soil moisture, and the top of the container was sealed with a rubber membrane. Soils without As(V)-Fh were used as the control group. The cultivation period was a total of 360 days.

### 2.5. DGT Preparation, Deployment and Calculation

A Chelex-Metsorb mixed binding layer (MBL)–DGT probe was purchased from DGT Research Ltd., Lancaster, UK. This DGT probe can simultaneously measure the variations in labile Fe and As in water, soil, or sediment. The window size of the MBL-DGT probe was 120 mm (length) × 18 mm (width). The MBL-DGT probe was deployed vertically at a distance of 2–3 mm from the nylon mesh column at 0, 60, 180, and 360 days. After the DGT probe was deployed for 24 h, it was carefully removed, and the soil covering its window surface was washed off with Milli–Q water. Then, the device was carefully opened; the binding gel was removed and cut into 24 pieces at 5 mm intervals in the vertical direction,

and each DGT slice was numbered. The slices were first eluted with 1 mL of 1 M $HNO_3$ for 24 h. Then, the gel was removed and washed repeatedly with Milli–Q water. Then, each slice was eluted with 1 mL of 1 M NaOH for 24 h, followed by elution with 1 M $HNO_3$. Then, the two groups of eluents were mixed, and the concentrations of iron and As in the extracts were determined via inductively coupled plasma–mass spectrometry (ICP–MS).

### 2.6. Determination of Soil pH and Eh

The pH and Eh of the soil column were determined using a clean pH 200 solid penetration pH (Eh) meter. The pH and Eh values of the 0–15 cm soil column under two moisture conditions, 70% SWHC and 120% SWHC, were measured on days 0, 60, 180, and 360. During analysis, the surface of the soil was pierced, and the values were allowed to stabilize for 4–5 min within each 1 cm interval before the pH and Eh data were read at depths of 0 to 15 cm.

### 2.7. Spectral Analysis of As(V)-Fh

After removing the DGT probe, the nylon mesh bag was removed from the soil in order to wash the soil off its surface. Then, the nylon mesh bag was cut with a ceramic blade at intervals of 3 cm, and the intervals were marked according to depth. Afterwards, the nylon mesh bag was carefully opened, and the As(V)-Fh was removed and rinsed with Milli–Q water. The samples were freeze-dried, and some samples were taken for spectral analysis. As(V)-Fh, buried at soil depths of −2.5 to −5.5 cm (surface soil) and of −11.5 cm to −14.5 cm (bottom soil), was selected for spectral characterization. The spectral characterization of As(V)-Fh was performed according to Zhang et al. [25], as described in Text S3 [27,28].

### 2.8. QA/QC

The water content of the incubation system was maintained by weighing the mass of the container once every three days. All glassware and core sediment samplers were soaked in 10% $HNO_3$ for at least 24 h, and then carefully treated with Milli-Q water. The deployment of the DGT probes and the storage of the sediment cores were performed in an anaerobic glovebox (96% $N_2$/4% $H_2$) to ensure that no oxygen was introduced into the soil. For the ICP–MS analysis, indium (In), rhodium (Rh), and rhenium (Re) were added at a mixed concentration of 10 μg/L as internal standards for ICP–MS analysis. A known concentration of Fe and As solution (20 μg/L) was used as an external standard for ICP–MS analysis. The recoveries of the internal standards and external standard were greater than 93.6% and 95.4%, respectively, throughout the whole detection process.

## 3. Results

### 3.1. Release of DGT-Labile Fe (DGT-Fe) in the Soil Vertical Pattern

The variations in DGT-Fe at 70% SWHC and 120% SWHC without As(V)-Fh addition are shown in Figure S2. After 360 days of incubation, DGT-Fe still maintained a relatively low level. The variations in DGT-Fe at 70% SWHC with respect to the As/Fe molar ratio of As(V)-Fh over time along the soil vertical profile are shown in Figure 1A,B. For the 0.05 As/Fe molar ratio, the concentration of DGT-Fe in the soil column increased from −2.5 cm (0.23 mg/L) to −14.5 cm (0.48 mg/L), but the overall concentration remained low after 0 days. After 180 and 360 days of incubation, the concentration of DGT-Fe in each soil layer still increased, and the concentration of DGT-Fe also slowly increased with increasing soil depth. At 360 days, at a soil depth of −2.5 to −5.5 cm, the concentration of DGT-Fe was 2.97 mg/L, approximately 11 times that observed at 0 days. Similarly, the average concentration of DGT-Fe at a depth of −11.5 to −14.5 cm was 3.57 mg/L, which was approximately 8 times greater than that at 0 days. Soil treated with an As/Fe molar ratio of 0.005 also showed a similar trend as that of the 0.05 As/Fe molar ratio group. The DGT-Fe concentration exhibited an increasing trend at various soil depths at 60, 180, and 360 days and gradually increased with increasing depth. Overall, after 360 days of

cultivation under 70% SWHC, although the DGT-Fe concentrations in the surface and bottom soil layers increased significantly compared to those at 0 days, the concentrations remained relatively low. In addition, there was no significant difference in the average concentration of DGT-Fe between the surface and bottom soil layers.
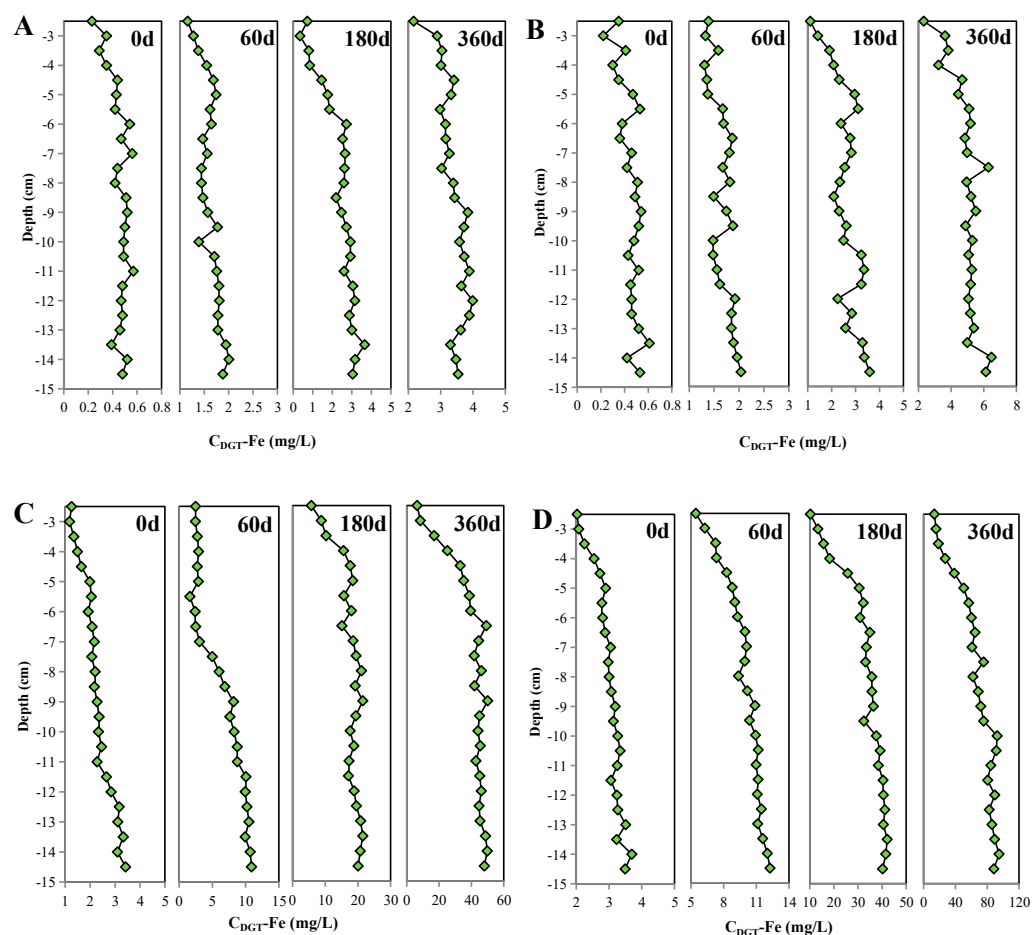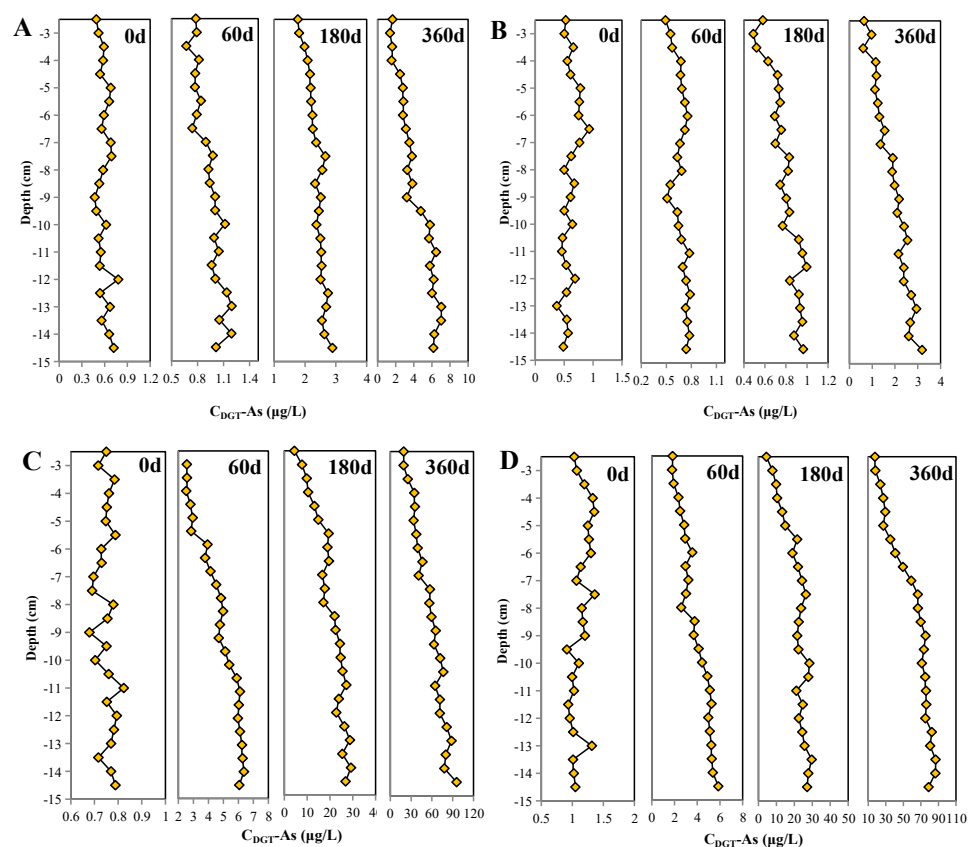


**Figure 1.** Changes in DGT-Fe concentrations in the soil vertical profile [(**A**) As(V)-Fh with a 0.05 As/Fe molar ratio under 70% SWHC treatment; (**B**) As(V)-Fh with a 0.005 As/Fe molar ratio under 70% SWHC treatment; (**C**) As(V)-Fh with a 0.05 As/Fe molar ratio under 120% SWHC treatment; (**D**) As(V)-Fh with a 0.005 As/Fe molar ratio under 120% SWHC treatment].

The variations in DGT-Fe in the soil vertical profile with different As/Fe molar ratios at 120% SWHC are shown in Figure 1C,D. For the 0.05 As/Fe molar ratio, the average concentration of DGT-Fe was 1.25 mg/L in the surface layer ($-2.5$ to $-5.5$ cm) and 3.42 mg/L in the bottom layer ($-11.5$ to $-14.5$ cm) at 0 days. At 60 days, the DGT-Fe concentration showed a significant upwards trend from the surface to the bottom layers, increasing from 2.46 mg/L to 10.89 mg/L. At 180 and 360 days, this trend became more pronounced. On day 360, the DGT-Fe concentration in the surface layer rapidly increased, with the average concentration increasing to 14.62 mg/L and 29.38 mg/L. The average concentrations of DGT-Fe in the bottom layer increased to 20.15 mg/L and 46.93 mg/L, indicating a significant increase compared to the values at 0 days and 60 days, respectively.

### 3.2. Release of DGT-Labile As (DGT-As) in the Soil Vertical Pattern

The variations in DGT-As at 70% SWHC and 120% SWHC without As(V)-Fh addition are shown in Figure S3. Similar to DGT-Fe, in the arsenic-uncontaminated soil, the DGT-As concentration remained much lower during the whole incubation for 360 days. Figure 2A,B shows the variation in DGT-As concentration under 70% SWHC at different As/Fe molar ratios in the soil vertical profile over time. For the 0.05 As/Fe molar ratio As(V)-Fh, the

overall concentration of DGT-As was low in the soil vertical profile. At 60 days, there were no significant changes in the DGT-As concentration compared to that at 0 days, and the DGT-As concentration only slightly increased from top to bottom. Similar trends were observed at 180 and 360 days, at which time DGT-As exhibited a steady upwards trend from the top to the bottom. Especially in the bottom layer, there was a significant change at 360 days compared to the level seen on day 0, when the average concentration increased from 0.79 to 6.53 µg/L (−11.5 to −14.5 cm), indicating that the concentration increased more than 8 times. Nevertheless, the concentration of DGT-As was still relatively low at a 0.05 As/Fe molar ratio As(V)-Fh under 70% SWHC. For the 0.005 As/Fe molar ratio As(V)-Fh, the concentration of DGT-As showed a similar trend as that of the high molar ratio at 0 and 60 days. No significant changes in DGT-As were observed in the soil vertical profile. However, there was a continuous upwards trend from the top to the bottom at 180 and 360 days. The average concentrations of DGT-As in the bottom layer from −11.5 to −14.5 cm were 0.95 µg/L and 2.87 µg/L, respectively, which were approximately 2 and 5 times greater than those at 0 days. In general, under 70% SWHC, the concentration of DGT-As under the two different As/Fe molar ratios did not change significantly throughout the whole 360-day period of incubation.
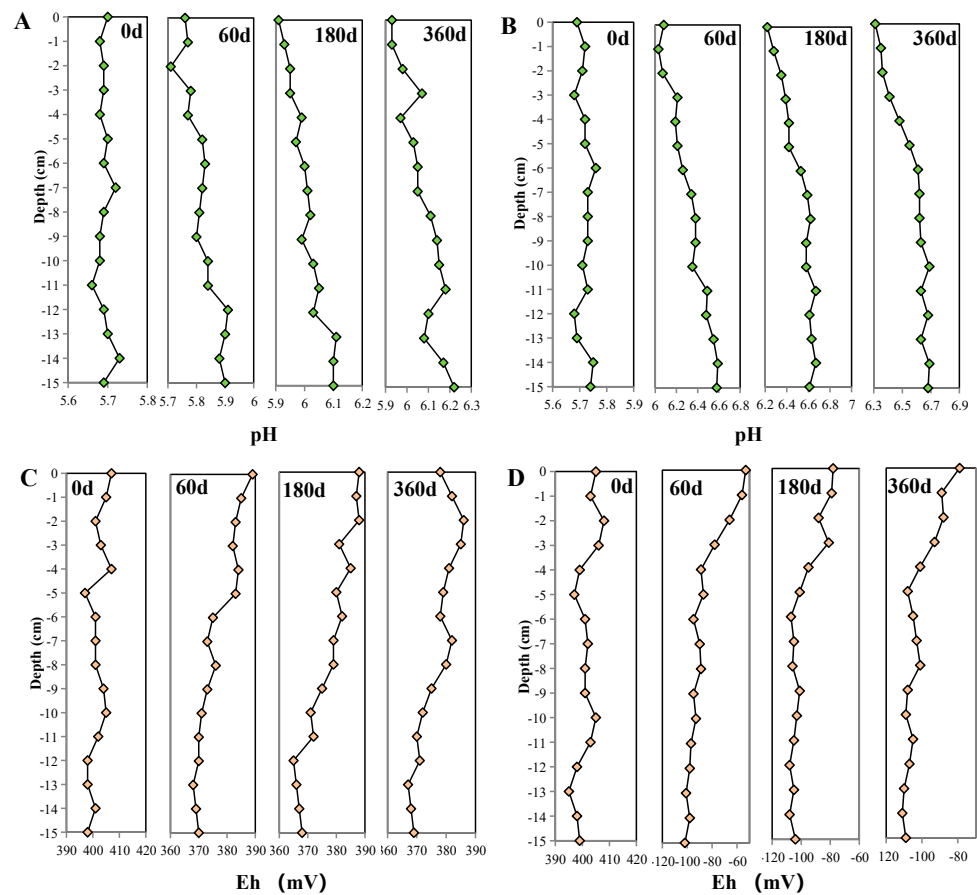


**Figure 2.** Changes in DGT-As in the soil vertical profile [(**A**) As(V)-Fh with a 0.05 As/Fe molar ratio under 70% SWHC treatment; (**B**) As(V)-Fh with a 0.005 As/Fe molar ratio under 70% SWHC treatment; (**C**) As(V)-Fh with a 0.05 As/Fe molar ratio under 120% SWHC treatment; (**D**) As(V)-Fh with a 0.005 As/Fe molar ratio under 120% SWHC treatment].

Figure 2C,D shows the changes in DGT-As under 120% SWHC in As(V)-Fh soil with different As/Fe molar ratios over time and along the vertical profile. In contrast to that at 0 days, the concentration of DGT-As under both treatments showed a continuous upwards trend from the surface to −2.5 cm and from the bottom to −14.5 cm during the 60 days of incubation. At 180 days and 360 days, the DGT-As still exhibited an increasing trend from the surface to the bottom. At the end of 360 days, the average concentrations of DGT-As in the surface layer from −2.5 cm to 5.5 cm reached 31.82 µg/L (0.05 As/Fe) and

26.59 µg/L (0.005 As/Fe), with average concentrations in the bottom layer from −11.5 to −14.5 cm reaching 87.13 µg/L (0.05 As/Fe) and 80.42 µg/L (0.005 As/Fe). By comparing the variations in DGT-Fe and DGT-As under 120% SWHC, it can be seen that DGT-Fe and DGT-As exhibited relatively similar variation processes in the soil vertical profile during the incubation period. However, the concentration of DGT-Fe tended to stabilize after 180 days, while that of DGT-As still exhibited an increasing trend, indicating that the dissociation and release of As from As(V)-Fh may have occurred later than that from iron. In addition, comparing the results at 70% and 120% SWHC indicated that, under a high-water content, the concentrations of DGT-Fe and DGT-As were significantly greater in the 120% SWHC treatment during the 360 days of incubation.

### 3.3. Changes in Soil pH and Reduction Potential (Eh) with Time

The changes in pH and soil Eh under different water conditions in the soil vertical profile are shown in Figure 3. The pH under the two different water conditions fluctuated in the soil vertical profile. After 70% SWHC, compared with the pH at 0 days, the soil pH increased by approximately 0.22–0.35 units at 60 days in the vertical soil profile (Figure 3A). Compared to the value at 60 days, the increasing trend was not obvious at 180 and 360 days: the pH increased by only 0.23–0.32 units, and the soil pH was 5.76–5.90. Under 120% SWHC, the soil pH significantly increased for 60 days, with a pH increase of 0.35–0.89 units and a 6.03–6.58 range in the soil vertical profile (Figure 3B). As for for 70% SWHC, the pH did not significantly increase at 180 and 360 days, but increased by only 0.11–0.24 units at 360 days in comparison to that at 60 days, and the final pH was 6.31–6.68 in the soil vertical profile.



**Figure 3.** Changes in soil pH and Eh with incubation time under different soil moisture conditions ((**A**) pH of the soil vertical profile under 70% SWHC treatment; (**B**) pH of the soil vertical profile under 120% SWHC treatment; (**C**) Eh of the soil vertical profile under 70% SWHC treatment; (**D**) Eh of the soil vertical profile under 120% SWHC treatment).

The changes in Eh under 70% SWHC are shown in Figure 3C. On day 0, the soil was in a highly aerobic state, and the soil Eh in the vertical profile was approximately 400 mV. After 360 days of incubation, the soil Eh slightly decreased, with Eh values ranging from 369 to 386 mV. There was a significant difference in Eh values between the 120% SHWC treatment and 70% SWHC treatment (Figure 3D). At 60 days, the soil Eh decreased from an initial 400 mV to −53−−102 mV. At 180 and 360 days, the changes in Eh maintained a high increasing trend in the surface layer, while Eh remained stable in the −102−−110 mV range at the bottom (−15 cm).

### 3.4. XRD Analysis of As(V)-Fh with Incubation Time

The transformation of poorly crystalline As(V)-Fh under 70% moisture conditions with incubation time was studied by XRD, as shown in Figure 4. Figure 4A shows that, for As(V)-Fh (0.05 As/Fe molar ratio), two standard peaks corresponding to ferrihydrite were observed at 41° (d ≈ 2.6 Å) and 75° (d ≈ 1.5 Å) at 0 days. At 60 and 180 days, only a small amount of hematite was generated in the surface layer (−2.5 to −5.5 cm) of As(V)-Fh (36°, 38° and 58°), but at 360 days, additional characteristic peaks corresponding to hematite (at 28°, 36°, 38°, 42°, 50°, 58°, 62° and 64°) were observed in the XRD pattern. Some of the peak areas and heights increased substantially, which indicated that more As(V)-Fh was transformed into hematite during the 360 days in the surface soil layer (5.8% hematite relative to the total components; Figure S4A). In the bottom layer (−11.5 to −14.5 cm), As(V)-Fh also transformed into hematite after 180 and 360 days of incubation (Figure 4B) (2.9% and 6.6%, respectively, relative to the total components; Figure S4B). In addition, the XRD characteristic peak of goethite was not found in the surface or bottom soil layers under the 70% SWHC treatment.
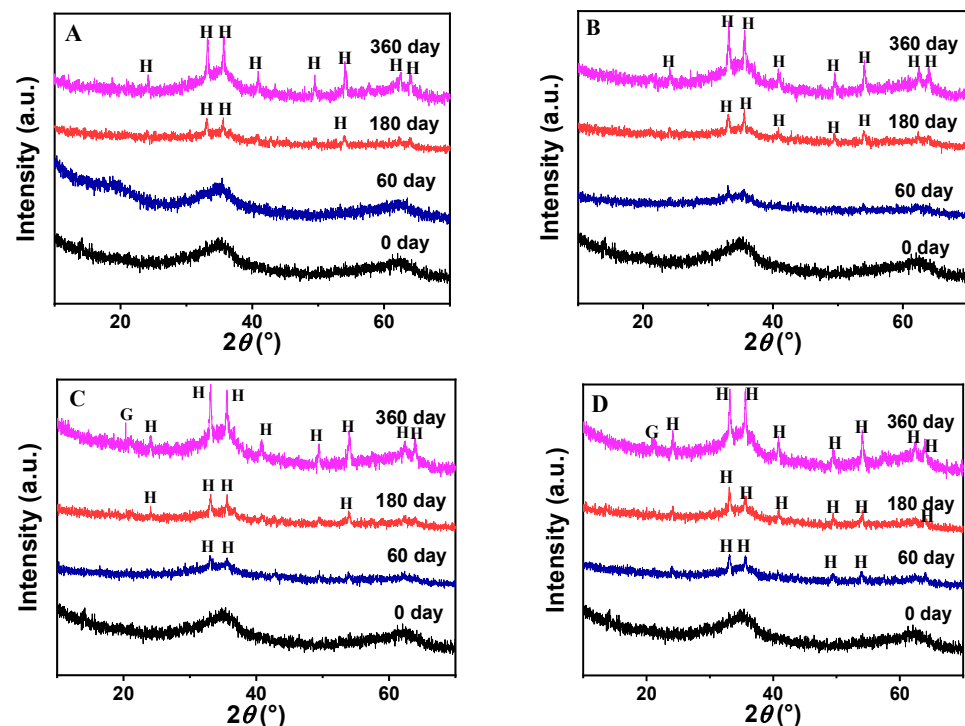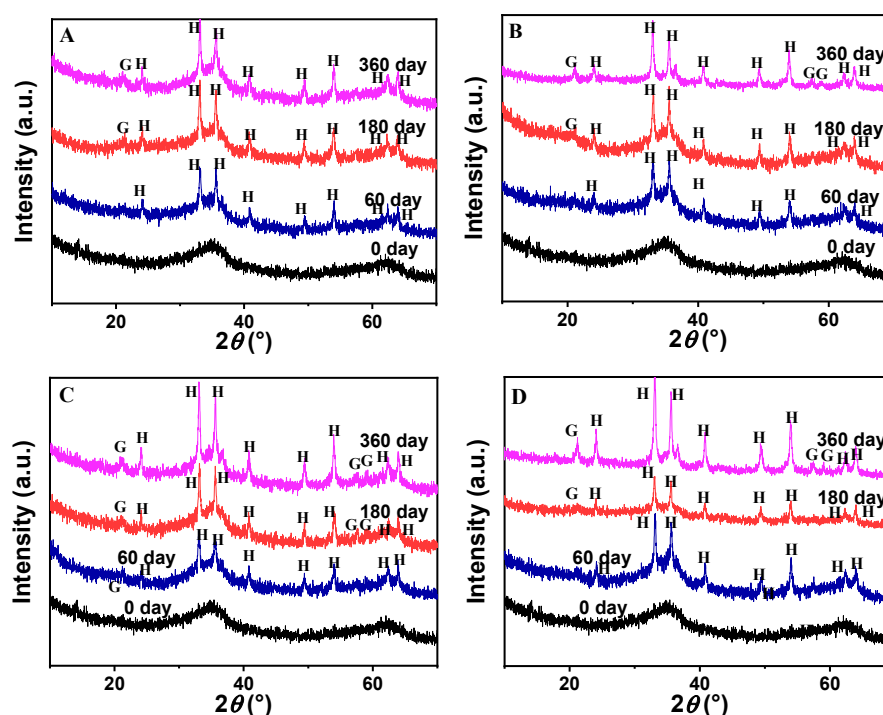


**Figure 4.** Changes in the XRD patterns of As(V)-Fh under 70% SWHC treatment after incubation for different durations ((**A**) As/Fe molar ratio = 0.05, −2.5−−5.5 cm soil layer; (**B**) As/Fe molar ratio = 0.05, −11.5−−14.5 cm soil layer; (**C**) As/Fe molar ratio = 0.005, −2.5−−5.5 cm soil layer; (**D**) As/Fe molar ratio = 0.005, −11.5−−14.5 cm soil layer).

The transformation of As(V)-Fh in the surface and bottom soil layers at a ratio of 0.005 As/Fe is shown in Figure 4C,D. In contrast to those in the high As/Fe molar ratio group, hematite peaks appeared earlier after 60 days of incubation, and a weak goethite sig-

nal peak was found for the first time after 360 days of incubation. We formed approximately 1.2% and 2.5% goethite in the surface and bottom soil layers, respectively (Figure S4C,D), indicating that goethite may still form after long-term As(V)-Fh incubation under low SWHC and a low As/Fe ratio.

The transformations of As(V)-Fh with respect to incubation time and the proportions of various minerals at 120% SWHC are shown in Figure 5 and Figure S5. In the −2.5 to −5.5 cm surface layer (Figure 5A,C), characteristic peaks of hematite appeared after 60 days of incubation. The peak heights and peak areas at 180 days and 360 days were much greater than those at 60 days. The proportion of hematite reached 23.40% and 11.40% under 0.005 As/Fe and 0.05 As/Fe molar ratios, respectively, at a −2.5−−5.5 cm soil depth after 360 days of incubation (Figure S5A,C). In addition, the characteristic peak of goethite appeared at 180 days under a high As/Fe ratio, but this peak was not found in the 70% SWHC sample. At 360 days, the proportions of goethite were 4.40% and 1.60% under 0.005 As/Fe and 0.05 As/Fe molar ratios, respectively, in the −2.5−−5.5 cm soil surface layer. Compared with those in the surface layer, more characteristic peaks of hematite and goethite appeared at a soil depth of −11.5−−14.5 cm, and the peaks were larger, wider, and sharper (Figure 5B,D). At this depth, 25.80% and 13.20% hematite and 5.70% and 2.10% goethite were formed over 360 days, respectively (Figure S5B,D). The above XRD results suggested that the long-term cultivation of soil under high-moisture conditions can promote the transformation of As-bearing ferrihydrite into hematite and goethite. In addition, the high As/Fe molar ratio inhibited the transformation of ferrihydrite to some extent, which indicates that the adsorption of a high amount of As may have a protective effect on ferrihydrite.



**Figure 5.** Changes in X-ray diffraction patterns of As-bearing hematite under 120% SWHC treatment after incubation for different durations ((**A**) As/Fe molar ratio = 0.05, −2.5−−5.5 cm soil layer; (**B**) As/Fe molar ratio = 0.05, −12.5−−14.5 cm soil layer; (**C**) As/Fe molar ratio = 0.005, −2.5−−5.5 cm soil layer; (**D**) As/Fe molar ratio = 0.005, −12.5−−14.5 cm soil layer).

### 3.5. SEM Analysis of As(V)-Fh with Respect to Incubation Time

Determining the surface morphology changes in As(V)-Fh by using scanning electron microscopy (SEM) can provide additional evidence of As(V)-Fh transformation. As shown in Figure S6, the initial As(V)-Fh before incubation showed the smooth clustering of small

particles. At 70% SWHC, As(V)-Fh with a 0.05 As/Fe molar ratio still presented smooth and uniform fine-particle clusters (Figure 6A,D) in the surface and bottom layers after 60 days of incubation. However, after 180 days of incubation, hematite with a shell shape began to appear (Figure 6B,E), and an increased amount of clearly defined hematite (Figure 6C,F) appeared at 360 days. The variation in As(V)-Fh over time at an As/Fe molar ratio of 0.005 was similar to that observed for a 0.05 As/Fe ratio. Hematite was also observed in the surface layer after 180 days and 360 days of incubation, while hematite was observed earlier, at 60 days, in the bottom layer. This result indicates that, at a low As/Fe molar ratio, the conversion rate of ferrihydrite will increase; these results are essentially consistent with the XRD results for the 70% SWHC group.
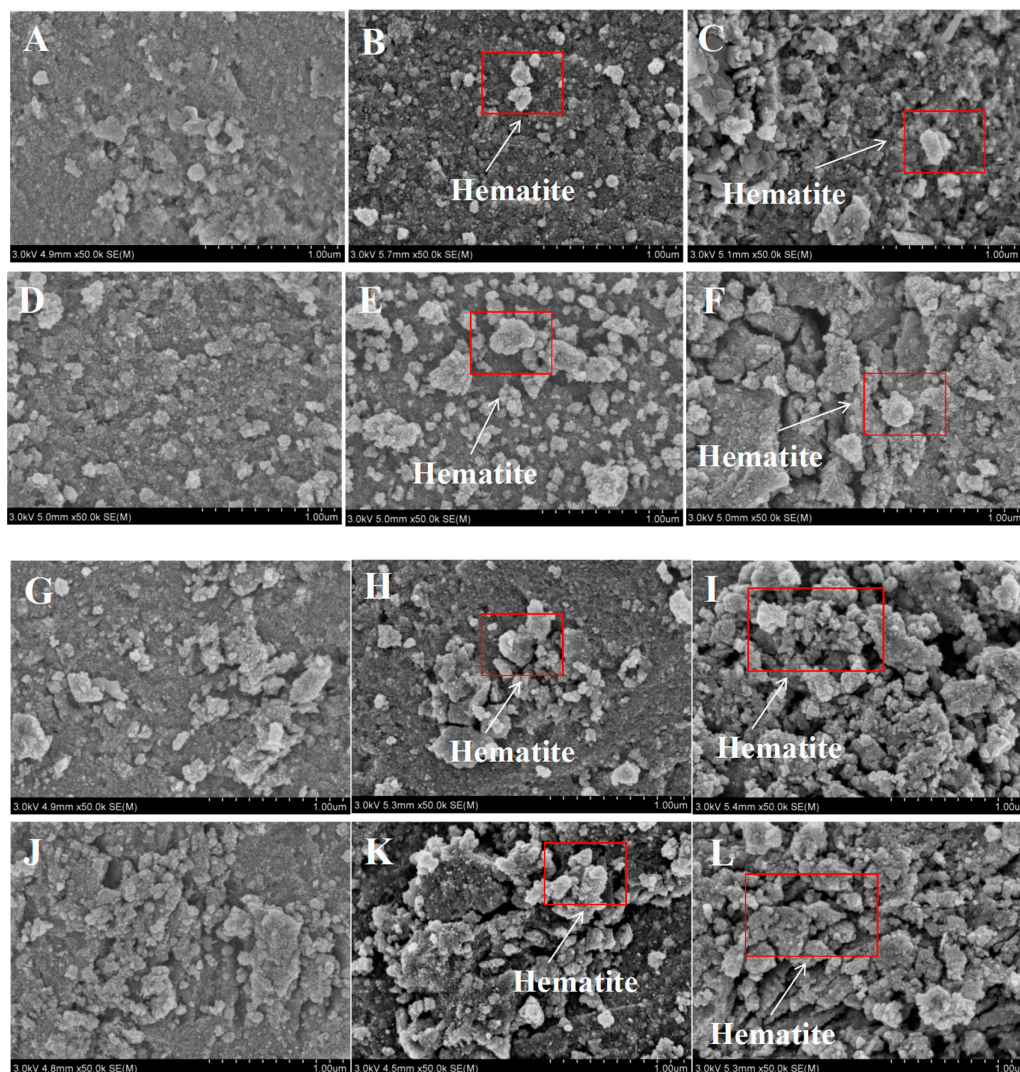


**Figure 6.** Surface morphology changes in As(V)-Fh under 70% SWHC treatment after different incubation times [the morphological changes in As(V)-Fh at 60 days, 180 days, and 360 days for (**A–C**); the same below; As/Fe molar ratio = 0.05, −2.5−−5.5 cm soil layer; (**D–F**): As/Fe molar ratio = 0.05, −11.5−−14.5 cm soil layer; (**G–I**): As/Fe molar ratio in the −2.5−−5.5 cm soil layer; (**J–L**): As/Fe molar ratio = 0.005, −11.5−−14.5 cm soil layer].

The surface morphology changes in As(V)-Fh under 120% SWHC are shown in Figure 7. After 60 days of incubation, As(V)-Fh (0.05 As/Fe molar ratio) taken from the surface and bottom soil layers exhibited a small number of hematite clusters (Figure 7A,D), and an increased amount of clearly defined hematite appeared at 180 days (Figure 7B,E). This sample was substantially different from the 70% SWHC sample seen at 360 days; a

clear and fine "rod-like" morphology of goethite was observed, and goethite was mixed with hematite clusters. Although the size of the goethite particles was not large at 360 days, electron microscopy still revealed clear evidence of goethite formation in As(V)-Fh under high-moisture conditions and a high As/Fe molar ratio. Compared with As(V)-Fh, which had a 0.05 As/Fe molar ratio, goethite appeared earlier, at 180 days, and a clearer morphology of goethite could be observed at 360 days. The goethite at 360 days was clearer and longer, with an obvious "needle-like" shape, and an independent goethite phase could be observed under the electron microscope. In summary, the SEM results further corroborate the XRD evidence related to hematite and goethite and confirm that the formation of goethite is probable under high-moisture conditions (anaerobic soil environment).
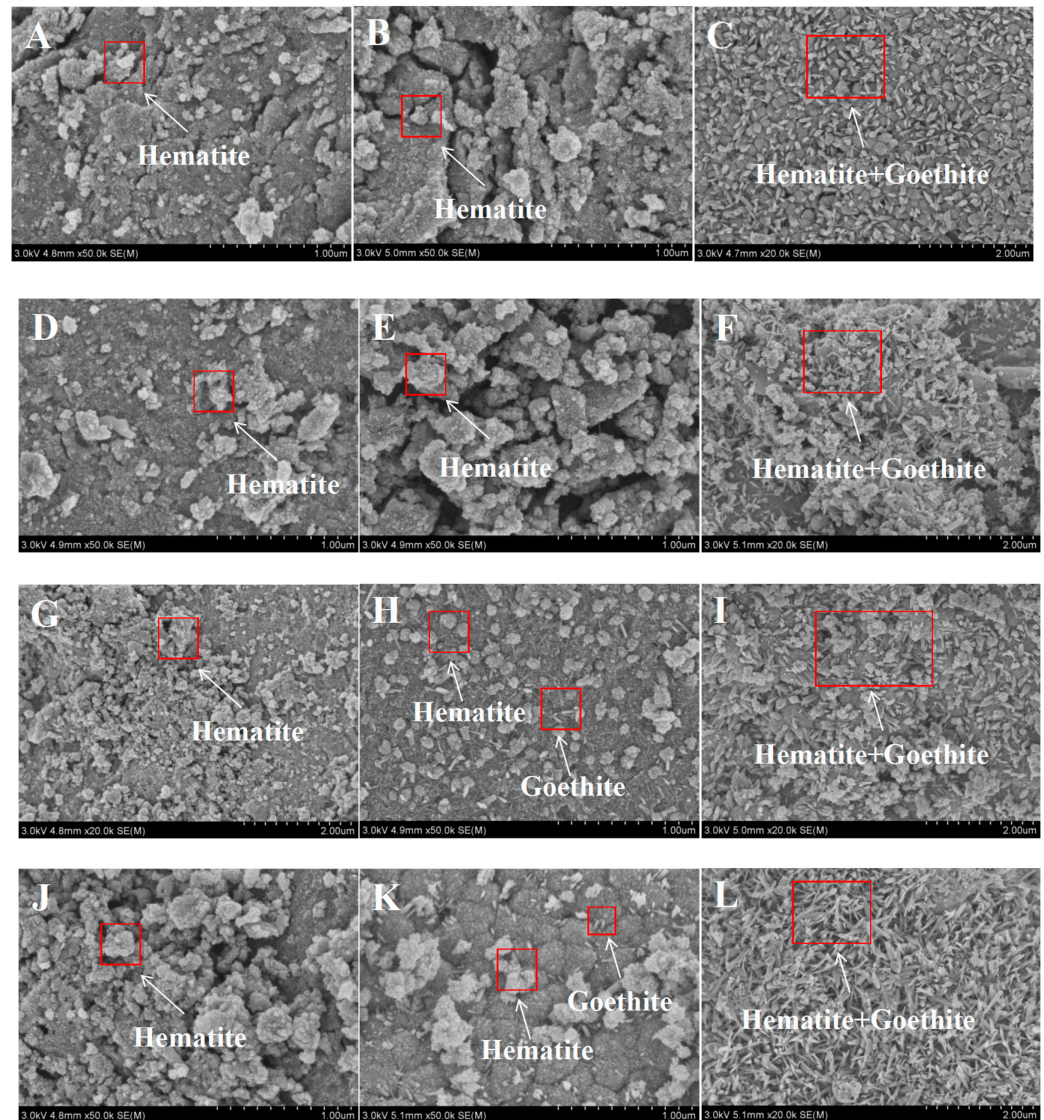


**Figure 7.** Surface morphology changes in As(V)-Fh under 120% SWHC treatment after different incubation times [morphology changes in As(V)-Fh at 60 days, 180 days, and 360 days for (**A–C**); As/Fe molar ratio = 0.05, −2.5−−5.5 cm soil layer; (**D–F**): As/Fe molar ratio = 0.05, −11.5−−14.5 cm soil layer; (**G–I**): As/Fe molar ratio in the −2.5−−5.5 cm soil layer; (**J–L**): As/Fe molar ratio = 0.005, −11.5−−14.5 cm soil layer].

### 3.6. Changes in the Specific Surface Area of As(V)-Fh with Incubation Time

The changes in the specific surface area of As(V)-Fh are shown in Table S2. Under the 70% SWHC treatment, the specific surface area of As(V)-Fh (0.05 As/Fe molar ratio) decreased by approximately 50 $m^2$/g ($-2.5$ to $-5.5$ cm) and 62 $m^2$/g ($-11.5$ to $-14.5$ cm) at 360 days. Like the variation in the 0.05 As/Fe molar ratio, the specific surface area decreased by approximately 62 $m^2$/g ($-2.5$ to $-5.5$ cm) and 79 $m^2$/g ($-11.5$ to $-14.5$ cm) at a 0.005 As/Fe molar ratio during 360 days of incubation. This indicates that the specific surface area of As(V)-Fh can continue to decrease even after incubating for a long time under low-soil-moisture conditions, possibly due to the formation of hematite, as mentioned above.

Compared to that of the 70% SWHC treatment, the specific surface area of As(V)-Fh in the 120% SWHC treatment dramatically decreased after 360 days of incubation, regardless of the As/Fe molar ratio. Especially for As(V)-Fh with a 0.005 molar ratio, the specific surface area of the soil surface layer decreased by nearly 179 $m^2$/g, a decrease of more than 50%. In the bottom soil layer, the specific surface area decreased by approximately 214 $m^2$/g, a decrease of more than 63%. This result was also consistent with the relevant XRD and SEM results mentioned above.

### 3.7. Changes in the Coordination Complexation and Valence States of Elements on the As(V)-Fh Surface

To further illuminate the potential transformation mechanism of As(V)-Fh in soil, we selected As(V)-Fh (0.005 As/Fe molar ratio) under 120% SWHC in the bottom soil layer ($-11.5$–$-14.5$ cm) as an example and analyzed the changes in the surface element coordination and valence states of As(V)-Fh by using XPS. As shown in Figure 8A, after 60 days of incubation, the characteristic peaks of As(V) and As(III) appeared at 42.5 and 45.32 eV, respectively. At 60 days, As(V) was still the dominant As phase on the mineral surface, with its peak area accounting for 93.93% and the As(III) peak area accounting for only 6.17%. However, the As(III) content gradually increased with continuous incubation, and the characteristic peak area of As(III) increased to 17.39% at 180 days and 35.15% at 360 days. As shown in Figure 8B, the 2p orbital characteristic peak of Fe mainly appeared at 710–725 eV. After 60 days of incubation, the characteristic peak area of Fe(II) on the surface of As(V)-Fh was 52.36%, and the characteristic peak area of Fe(III) reached 47.64%. After 180 and 360 days of cultivation, the characteristic peak areas of Fe(II) reached 61.80% and 75.25%, respectively. This suggested that, after 360 days of incubation, the main form of Fe on the As(V)-Fh surface was Fe(II). These findings and the As XPS results indicate that the flooded-soil environment significantly promoted the reduction of As(V) and Fe(III) on the As(V)-Fh surface.

The O 1s XPS spectrum is shown in Figure 8C. This full spectrum can be divided into three characteristic peaks, corresponding to Fe-O-Fe (530 eV), Fe-O-H or Fe-O-As (531.4 eV), and surface-adsorbed water ($H_2O$) (532.9 eV) [29,30]. With long-term incubation under flooded conditions, the characteristic peak area of Fe-O-Fe gradually increased. At 60 days, the characteristic peak area of Fe-O-Fe was 42.48%, and this area increased to 58.63% at 360 days. This result indicated that the Fe content adsorbed onto the mineral surface increased, and that additional Fe-O-Fe structured minerals were formed. In contrast, the proportions of Fe-O-H (As) (which decreased from 45.47% at 60 days to 33.93% at 360 days) and adsorbed $H_2O$ (which decreased from 11.95% at 60 days to 7.45% at 360 days) presented obvious decreasing trends. This indicated that As was gradually released from the surface of As(V)-Fh during continuous incubation. In addition, the decrease in adsorbed $H_2O$ further indicated that dehydration and dehydrogenation occurred during the transformation of ferrihydrite into hematite, leading to the reduction of surface OH groups [28,31].
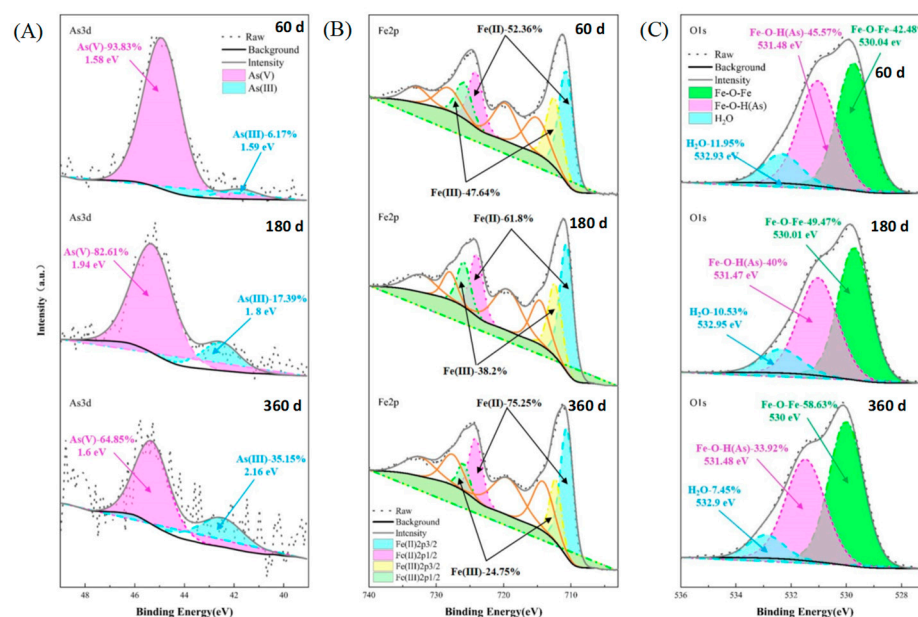
**Figure 8.** Changes in the XPS 3d (**A**), iron 2p (**B**), and oxygen 1s (**C**) spectra after As(V)-Fh incubation in the soil for 360 days.

## 4. Discussion

### 4.1. Transformation of As-Bearing Ferrihydrite in Soil

In recent years, extensive research has been conducted on the conversion of ferrihydrite or As-bearing ferrihydrite, but most of these studies have been limited to mechanistic research in aqueous systems [18,32,33]. The soil matrix is more complex than a pure-solution system, and soil moisture may play an important role in the transformation and fate of As-bearing ferrihydrite in soil. Thus, it is important to study the transformation process of As-bearing ferrihydrite at different soil moisture levels and clarify how soil moisture affects transformation products and the mechanism of As remobilization. Based on the DGT and spectral analysis results, we obtained clear evidence of the transformation of As-bearing ferrihydrite into crystalline iron oxides under long-term-submerged and highly aerobic or anaerobic environmental conditions. The XRD and SEM results showed that, in the present study, the main product of transformed As(V)-Fh was hematite under both low-soil-moisture (70% SWHC) and flooded-soil (120% SWHC) conditions. With increasing soil depth and incubation time, more hematite is produced. The formation of hematite is mainly due to the gradual decrease in the pH of red soil during long-term incubation. Previous studies have shown that hematite is formed via dehydration and the internal atomic arrangement of ferrihydrite at near-neutral pH (6–8) [28,31,34]. The XPS results in this study further explained the key mechanism involved in the formation of hematite. Figure 8 shows that, during 360 days of incubation, the amount of Fe-O-H(As) on the surface of As(V)-Fh decreased significantly, while the content of Fe-O-Fe groups increased. Dehydrogenation and the formation of new Fe-O-Fe bonds indicated that As(V)-Fh underwent atomic rearrangement to form hematite. In addition, the XPS results showed that the content of $H_2O$ on the As(V)-Fh surface decreased, which further indicated that the dehydration process of As(V)-Fh led to the formation of hematite.

In this study, the XRD results also showed that As(V)-Fh transformed into goethite, especially under 120% SWHC (flooded conditions). This difference is probably caused by Fe(II), which may catalyze the reductive dissolution of ferrihydrite in soil and its subsequent transformation into goethite. In the soil environment, long-term flooding can lead to the gradual reduction of Fe(III) in the soil solution to Fe(II) [35,36]. As shown in Figure 1, the concentration of Fe(II) measured by the DGT probe did not change significantly throughout the whole 360 days under the 70% SWHC treatment, but the concentration gradually increased with soil depth and incubation time under the 120% SWHC

treatment. Previous studies have shown that Fe(II) is the key factor and catalyst that significantly promotes the transformation of ferrihydrite or As-bearing ferrihydrite into goethite and lepidocrocite [37,38]. Although most of the reported research involved aqueous environments, this study further proved that Fe(II) may be the key to the transformation of As-bearing ferrihydrite into goethite in a flooded-soil environment through buried nylon bag experiments. This process is mainly realized through direct electron transfer and atom exchange processes between Fe(II), with its increasing concentration in the soil solution, and Fe(III) present on the surface of As(V)-Fh. After the Fe(II) present in soil solutions adsorbs onto the surface of As(V)-Fh, the As(V)-Fh provides electrons to the iron, which is oxidized to Fe(III). This material serves as the structural component of the secondary iron oxide mineral formed in the soil. The provided electrons are transmitted through solid-state electron conduction to structural Fe(III) at other positions in As(V)-Fh, causing Fe(III) reduction and its subsequent dissolution/release to the surface or into the solution of As(V)-Fh, forming free Fe(II) [38,39]. Notably, during this reaction process, there was no change in the total amount of free Fe (including dissolved and adsorbed Fe) or the amount of structural Fe in the soil solution. However, exchange occurs between free Fe and structural Fe. During the exchange process, As(V)-Fh undergoes a transformation process [40], which ultimately leads to the dissociation of As(V)-Fh under reducing conditions and the reorganization of Fe(III) into new mineral forms (goethite). The Fe 2p XPS spectra in this study further proved that Fe(II) gradually accumulated on the surface of the minerals with increasing incubation time. The increase in the intensity of the characteristic Fe(II) peak indicated that Fe(II) gradually adsorbed onto the surface of As(V)-Fh in the soil system and promoted the formation of goethite. In addition, according to the results of previous studies on the effect of the Fe(II) concentration and pH on the formation of ferrihydrite products, the low concentration of Fe(II) and increasing pH seen in this study are conducive to the formation of goethite. Several studies have shown that a high concentration of $Fe^{2+}$ is conducive to the formation of magnetite, while a low concentration is conducive to the formation of lepidocrocite and goethite. A continuous increase in pH during incubation also leads to the further accumulation of negative charges on the mineral surface and contributes to the attraction of $Fe^{2+}$ ions [38,41].

Previous aqueous system studies have shown that the structural stability of ferrihydrite significantly increases when As is adsorbed onto the outer surface or bound to the internal surface through bidentate mechanisms [15,42,43]. By comparing the results for the two molar ratios of As(V)-Fh, we found that the above phenomenon also occurred in the soil environment. The transformation of As(V)-Fh at a high molar ratio was significantly inhibited. Even in the bottom soil layer under flooded conditions, the concentration of DGT-Fe released from the dissociation of As(V)-Fh at a high molar ratio was several times lower than that released at a low molar ratio. In addition, the results of XRD, SEM, and Brunauer–Emmett–Teller (BET) analysis demonstrated that the crystallization of hematite and goethite was significantly inhibited. The Fe-O-As bonds formed by the adsorption of high amounts of As onto ferrihydrite are usually not easily replaced by Fe(II) or protons to form Fe-O-Fe or Fe-O-H, which inhibits the formation of new crystalline iron oxides. In addition, As(V) may occupy the adsorption sites of Fe(II) after adsorption and hinder electron conduction between Fe(II) and Fe(III) on the surface. Other studies have shown that, when As(V), Fe(II), and ferrihydrite coexist in a system, the ternary complex Fe(II)-As(V)-Fh may be formed, and As(V) hinders the chemical interaction between these three components [18]. However, this binding mode was not observed in the XPS results of this study, which was potentially related to the complex environmental system of soil and the low concentration of Fe(II) in the solution system. This also indicates that, when ferrihydrite is added to highly As-polluted soil environments, its stability may increase due to complex conditions and inhibit the release of As into the environment.

*4.2. Redistribution Process of As in Mineral and Soil Systems*

As may be released during the reductive dissolution or transformation of As-bearing ferrihydrite in aqueous solutions [15,18,41]. In the present study, we obtained similar results in the soil environment. The DGT results indicated that the concentration of DGT-As gradually increased with increasing incubation time and soil depth. A comparison of the results for the two SWHCs clearly reveals that, under flooded conditions, the release of As into the soil solution was particularly significant. Considering the results of BET-based specific surface area analysis, we suggest that the main reason for this difference is the significant decrease in specific surface area caused by the crystallization and recombination of As-bearing ferrihydrite. After treatment with a 0.005 As/Fe molar ratio under 120% SWHC, the specific surface area was only 110.21 $m^2/g$ at 360 days, a decrease of nearly three times. Newly formed hematite and goethite usually have larger grain sizes and smaller specific surface areas. This also indicates that, when As-bearing ferrihydrite undergoes transformation into stable crystalline minerals, the specific surface area decreases, accompanied by a decrease in the number of adsorption sites for As on the mineral surface, which can easily lead to the release of As into the soil solution. In addition, the results of XPS analysis showed that the reduction of As(V) into As(III) occurred on the mineral surface. This result also indicated that the free Fe(II) adsorbed onto the mineral surface may act as a reductant and electron donor for As(V) to generate As(III) through a redox reaction in a flooded anaerobic environment [33].

Based on the abovementioned results and conclusions, we clarified the dynamics of As-bearing ferrihydrite in the soil environment and determined the potential environmental risk of As release when ferrihydrite is used as a long-term amendment in a high-soil moisture environment. Thus, ferrihydrite application should be avoided in long-term-flooded soil, especially in the red soil region of South China. In addition, according to the results of the present study, we recommend a paddy–dry-field rotation pattern to guarantee the reasonable use of ferrihydrite as an effective amendment, namely, one season for rice growth (approximately 60–90 days of flooded soil) and one season for dryland plants, such as maize, wheat, or vegetable crops. This crop planting pattern may reduce the transformation of ferrihydrite into hematite and goethite to a large extent, thus avoiding the secondary release of As into the soil environment.

**5. Conclusions**

In this study, we used a spectral characterization technique combined with DGT to systematically investigate the fate of As-bearing ferrihydrite at different SWHCs and soil depths. The transformation rate of As(V)-Fh under 120% SWHC was significantly greater than that under 70% SWHC, and the transformation rate increased with increasing soil depth. The DGT results showed that As and Fe were released from As(V)-Fh in the saturated soil vertical profile after 60 days. Hematite and goethite were the main products and byproducts of the As(V)-Fh transformation process, respectively. The potential transformation mechanism determined via XPS revealed that As(V)-Fh mainly transformed into hematite through dehydrogenation and dehydration, and that the adsorption of Fe(II) generated from long-term-saturated soil onto As(V)-Fh was the key process catalyzing the nuclear recombination of As(V)-Fh and the generation of goethite. Ferrihydrite should be considered for use as an amendment for As remediation for more than 180 days in long-term-flooded red soil. Thus, we strongly recommend the application of ferrihydrite in paddy–dry rotation or dry-field patterns to prevent the loss of As(V)-Fh. Field drainage over time should also be considered during the rainy season.

**Supplementary Materials:** The following supporting information can be downloaded at https://www.mdpi.com/article/10.3390/agriculture14030450/s1, Text S1: Analysis of soil physicochemical properties; Text S2: Synthesis of As(V)-Fh; Text S3: Spectral characterization of As(V)-Fh; Figure S1: Soil incubation device; Figure S2: Changes in DGT-Fe in the soil vertical profile with no As(V)-Fh addition (A: 70%SWHC; B: 120%SWHC); Figure S3: Changes in DGT-As in the soil vertical profile with no

As(V)-Fh addition (A: 70%SWHC; B: 120%SWHC); Figure S4: Composition of As(V)-Fh under 70% SWHC moisture conditions after incubation for 360 days; Figure S5: Composition of As(V)-Fh under 70% SWHC moisture conditions after incubation for 360 days; Figure S6: Morphological characteristics of the original As-bearing ferrihydrite in unadded soil under scanning electron microscopy; Table S1: Basic physical and chemical properties of the tested soil; Table S2: Changes in the specific surface area of As-bearing ferrihydrite with incubation.

**Author Contributions:** L.L.: writing-original draft preparation; X.C.: investigation; Y.W.: software and data curation; F.Z.: supervision; X.Z.: investigation; T.Z., supervision. All authors have read and agreed to the published version of the manuscript.

**Institutional Review Board Statement:** Not applicable.

**Informed Consent Statement:** Not applicable.

**Data Availability Statement:** Data are contained within the article.

**Conflicts of Interest:** The authors declare no conflicts of interest.

## References

1. Hughes, M.F. Arsenic toxicity and potential mechanisms of action. *Toxicol. Lett.* **2002**, *133*, 1–16. [CrossRef]
2. Finnegan, P.M.; Chen, W. Arsenic toxicity: The effects on plant metabolism. *Front. Physiol.* **2012**, *3*, 182. [CrossRef]
3. Abdul, K.S.M.; Jayasinghe, S.S.; Chandana, E.P.; Jayasumana, C.; De Silva, P.M.C. Arsenic and human health effects: A review. *Environ. Toxicol.* **2015**, *40*, 828–846.
4. Ng, J.C.; Wang, J.; Shraim, A. A global health problem caused by arsenic from natural sources. *Chemosphere* **2003**, *52*, 1353–1359. [CrossRef]
5. Smedley, P.L.; Kinniburgh, D.G. A review of the source, behaviour and distribution of arsenic in natural waters. *Appl. Geochem.* **2002**, *17*, 517–568. [CrossRef]
6. Yim, S.R.; Park, G.Y.; Lee, K.W.; Chung, M.S.; Shim, S.M. Determination of total arsenic content and arsenic speciation in different types of rice. *Food Sci. Biotechnol.* **2017**, *26*, 293–298. [CrossRef] [PubMed]
7. World Health Organization. *Arsenic in Drinking-Water: Background Document for Development of WHO Guidelines for Drinking-Water Quality (No. WHO/SDE/WSH/03.04/75)*; World Health Organization: Geneva, Switzerland, 2003.
8. Michael, H.A. An arsenic forecast for China. *Science* **2013**, *341*, 852–853. [CrossRef] [PubMed]
9. Li, S.; Wang, W.; Liang, F.; Zhang, W.X. Heavy metal removal using nanoscale zero-valent iron (nZVI): Theory and application. *J. Hazard. Mater.* **2017**, *322*, 163–171. [CrossRef] [PubMed]
10. Wu, C.; An, W.; Liu, Z.; Lin, J.; Qian, Z.; Xue, S. The effects of biochar as the electron shuttle on the ferrihydrite reduction and related arsenic (As) fate. *J. Hazard Mater.* **2020**, *390*, 121391. [CrossRef] [PubMed]
11. Zhang, Z.; Moon, H.S.; Myneni, S.C.; Jaffé, P.R. Effect of dissimilatory iron and sulfate reduction on arsenic dynamics in the wetland rhizosphere and its bioaccumulation in wetland plants (*Scirpus actus*). *J. Hazard. Mater.* **2017**, *321*, 382–389. [CrossRef] [PubMed]
12. Shipley, H.J.; Engates, K.E.; Guettner, A.M. Study of iron oxide nanoparticles in soil for remediation of arsenic. *J. Nanopart. Res.* **2011**, *13*, 2387–2397. [CrossRef]
13. Matsumoto, S.; Kasuga, J.; Makino, T.; Arao, T. Evaluation of the effects of application of iron materials on the accumulation and speciation of arsenic in rice grain grown on uncontaminated soil with relatively high levels of arsenic. *Environ. Exp. Bot.* **2016**, *125*, 42–51. [CrossRef]
14. Peak, D.; Regier, T. Direct observation of tetrahedrally coordinated Fe (III) in ferrihydrite. *Environ. Sci. Technol.* **2012**, *46*, 3163–3168. [CrossRef]
15. Zhao, X.; Yuan, Z.; Wang, S.; Zhang, G.; Qu, S.; Wang, Y.; Liu, S.; Pan, Y.; Lin, J.; Jia, Y. The fate of co-existent cadmium and arsenic during Fe (II)-induced transformation of As (V)/Cd (II)-bearing ferrihydrite. *Chemosphere* **2022**, *301*, 134665. [CrossRef] [PubMed]
16. Fan, J.X.; Wang, Y.J.; Liu, C.; Wang, L.H.; Yang, K.; Zhou, D.M.; Li, W.; Sparks, D.L. Effect of iron oxide reductive dissolution on the transformation and immobilization of arsenic in soils: New insights from X-ray photoelectron and X-ray absorption spectroscopy. *J. Hazard. Mater.* **2014**, *279*, 212–219. [CrossRef]
17. Das, S.; Essilfie-Dughan, J.; Hendry, M.J. Fate of adsorbed arsenate during phase transformation of ferrihydrite in the presence of gypsum and alkaline conditions. *Chem. Geol.* **2015**, *411*, 69–80. [CrossRef]
18. Zhang, G.; Yuan, Z.; Lei, L.; Lin, J.; Wang, X.; Wang, S.; Jia, Y. Arsenic redistribution and transformation during Fe (II)-catalyzed recrystallization of As-adsorbed ferrihydrite under anaerobic conditions. *Chem. Geol.* **2019**, *525*, 380–389. [CrossRef]

19. Erbs, J.J.; Berquó, T.S.; Reinsch, B.C.; Lowry, G.V.; Banerjee, S.K.; Penn, R.L. Reductive dissolution of arsenic-bearing ferrihydrite. *Geochim. Cosmochim. Acta* **2010**, *74*, 3382–3395. [CrossRef]

20. Stolze, L.; Zhang, D.; Guo, H.; Rolle, M. Model-based interpretation of groundwater arsenic mobility during in situ reductive transformation of ferrihydrite. *Environ. Sci. Technol.* **2019**, *53*, 6845–6854. [CrossRef]

21. Yang, F.; Xie, S.W.; Wei, C.Y.; Liu, J.X.; Zhang, H.Z.; Chen, T.; Zhang, J. Arsenic characteristics in the terrestrial environment in the vicinity of the Shimen realgar mine, China. *Sci. Total Environ.* **2018**, *626*, 77–86. [CrossRef]

22. Wu, C.; Huang, L.; Xue, S.G.; Pan, W.S.; Zou, Q.; Hartley, W.; Wong, M.H. Oxic and anoxic conditions affect arsenic (As) accumulation and arsenite transporter expression in rice. *Chemosphere* **2017**, *168*, 969–975. [CrossRef]

23. Mallet, M.; Barthélémy, K.; Ruby, C.; Renard, A.; Naille, S. Investigation of phosphate adsorption onto ferrihydrite by X-ray photoelectron spectroscopy. *J. Colloid Interf. Sci.* **2013**, *407*, 95–101. [CrossRef]

24. Ding, Z.; Fu, F.; Dionysiou, D.D.; Tang, B. Coadsorption and subsequent redox conversion behaviors of As (III) and Cr (VI) on Al-containing ferrihydrite. *Environ. Pollut.* **2018**, *235*, 660–669. [CrossRef]

25. Zhang, T.; Chen, X.; Wang, Y.; Li, L.; Sun, Y.; Wang, Y.; Zeng, X. The stability of poorly crystalline arsenical ferrihydrite after long-term soil suspension incubation. *Chemosphere* **2022**, *291*, 132844. [CrossRef]

26. Cai, L.; Liu, G.; Rensing, C.; Wang, G. Genes involved in arsenic transformation and resistance associated with different levels of arsenic-contaminated soils. *BMC Microbiol.* **2009**, *9*, 1–11. [CrossRef]

27. Hu, S.W.; Lu, Y.; Peng, L.F.; Wang, P.; Zhu, M.Q.; Dohnalkova, A.C.; Chen, H.; Lin, Z.; Dang, Z.; Shi, Z. Coupled kinetics of ferrihydrite transformation and As(V) sequestration under the effect of humic acids: A mechanistic and quantitative study. *Environ. Sci. Technol.* **2018**, *52*, 11632–11641. [CrossRef]

28. Yang, Z.; Bai, L.; Su, S.; Wang, Y.; Wu, C.; Zeng, X.; Sun, B. Stability of Fe–As composites formed with As (V) and aged ferrihydrite. *J. Environ. Sci.* **2021**, *100*, 43–50. [CrossRef] [PubMed]

29. Ojeda, J.J.; Romero-Gonzalez, M.E.; Pouran, H.M.; Pouran, H.M. In situ monitoring of the biofilm formation of Pseudomonas putida on hematite using flow-cell ATR-FTIR spectroscopy to investigate the formation of inner-sphere bonds between the bacteria and the mineral. *Mineral. Mag.* **2008**, *72*, 101–106. [CrossRef]

30. Xue, Q.; Ran, Y.; Tan, Y.Z.; Peacock, C.L. Arsenite and arsenate binding to ferrihydrite organo-mineral coprecipitate: Implications for arsenic mobility and fate in natural environments. *Chemosphere* **2019**, *224*, 103–110. [CrossRef]

31. Yu, P.; Fu, F.; Sun, G.; Tang, B. Effects of oxalate and citrate on the behavior and redistribution of Cr (VI) during ferrihydrite-Cr (VI) co-precipitates transformation. *Chemosphere* **2021**, *266*, 128977. [CrossRef] [PubMed]

32. Kameda, K.; Hashimoto, Y.; Wang, S.L.; Hirai, Y.; Miyahara, H. Simultaneous and continuous stabilization of As and Pb in contaminated solution and soil by a ferrihydrite-gypsum sorbent. *J. Hazard. Mater.* **2017**, *327*, 171–179. [CrossRef]

33. Perez, J.P.H.; Tobler, D.J.; Thomas, A.N.; Freeman, H.M.; Dideriksen, K.; Radnik, J.; Benning, L.G. Adsorption and reduction of arsenate during the Fe$^{2+}$ -induced transformation of ferrihydrite. *ACS Earth Space Chem.* **2019**, *3*, 884–894. [CrossRef]

34. Liu, H.; Li, P.; Lu, B.; Wei, Y.; Sun, Y. Transformation of ferrihydrite in the presence or absence of trace Fe(II): The effect of preparation procedures of ferrihydrite. *J. Solid State Chem.* **2009**, *182*, 1767–1771. [CrossRef]

35. Malakar, A.; Kaiser, M.; Snow, D.D.; Walia, H.; Panda, B.; Ray, C. Ferrihydrite reduction increases arsenic and uranium bioavailability in unsaturated soil. *Environ. Sci. Technol.* **2020**, *54*, 13839–13848. [CrossRef]

36. Grigg, A.R.; ThomasArrigo, L.K.; Schulz, K.; Rothwell, K.A. Ferrihydrite transformations in flooded paddy soils: Rates, pathways, and product spatial distributions. *Environ. Sci. Proc. Imp.* **2022**, *24*, 1867–1882. [CrossRef]

37. Pedersen, H.D.; Postma, D.; Jakobsen, R. Release of arsenic associated with the reduction and transformation of iron oxides. *Geochim. Cosmochim. Acta* **2006**, *70*, 4116–4129. [CrossRef]

38. Zhao, X.; Yuan, Z.; Wang, S.; Pan, Y.; Chen, N.; Ayetullah, T.; Kalong, C.; Aslan, A.; Chen, W.; Reza, D.; et al. Iron (II)-activated phase transformation of Cd-bearing ferrihydrite: Implications for cadmium mobility and fate under anaerobic conditions. *Sci. Total Environ.* **2022**, *848*, 157719. [CrossRef] [PubMed]

39. Liu, C.; Li, F.; Chen, M.; Liao, C.; Tong, H.; Hua, J. Adsorption and Stabilization of Lead during Fe(II)-catalyzed Phase Transformation of Ferrihydrite. *Acta Chim. Sin.* **2017**, *75*, 621–628. (In Chinese) [CrossRef]

40. Handler, R.M.; Frierdich, A.J.; Johnson, C.M.; Rosso, K.M.; Beard, B.L.; Wang, C.; Latta, D.E.; Neumann, A.; Pasakarnis, T.; Premaratne, W.A.P.J.; et al. Fe (II)-catalyzed recrystallization of goethite revisited. *Environ. Sci. Technol.* **2014**, *48*, 11302–11311. [CrossRef]

41. Pedersen, H.D.; Postma, D.; Jakobsen, R.; Larsen, O. Fast transformation of iron oxyhydroxides by the catalytic action of aqueous Fe(II). *Geochim. Cosmochim. Acta* **2005**, *69*, 3967–3977. [CrossRef]

42. Das, S.; Essilfie-Dughan, J.; Hendry, M.J. Arsenate partitioning from ferrihydrite to hematite: Spectroscopic evidence. *Am. Mineral.* **2014**, *99*, 749–754. [CrossRef]

43. Michael Bolanz, R.; Bläss, U.; Ackermann, S.; Ciobotă, V.; Rösch, P.; Tarcea, N.; Popp, J.; Majzlan, J. The effect of antimonate, arsenate, and phosphate on the transformation of ferrihydrite to goethite, hematite, feroxyhyte, and tripuhyite. *Clays Clay Miner.* **2013**, *61*, 11–25. [CrossRef]